



Fabrication of metal-organic framework@Yeast composite materials for efficient removal of Pb²⁺ in water

Jinguli Wen, Panpan He, Chao Lei, Enjun Lv, Yuhang Wu, Junkuo Gao*, Juming Yao

Institute of Fiber Based New Energy Materials, The Key Laboratory of Advanced Textile Materials and Manufacturing Technology of Ministry of Education, College of Materials and Textiles, Zhejiang Sci-Tech University, Hangzhou 310018, China



ARTICLE INFO

Keywords:
Metal-organic frameworks
Yeast
In situ growth
Pb²⁺ adsorption

ABSTRACT

ZIF-67@Yeast was synthesized with in-situ growth procedure by using hydrothermally carbonized yeast as the substrate material. The prepared ZIF-67@Yeast was characterized in detail by SEM, BET, XRD and TG analysis. In addition, the adsorption properties of Pb²⁺ by ZIF-67@Yeast were also investigated. The results show that the adsorption capacity of Pb²⁺ by ZIF-67@Yeast is larger than the sum of the adsorption capacity of Pb²⁺ by individual yeast and ZIF-67. Yeast could maintain a stable morphology after hydrothermal carbonization at 180 °C. Therefore, many MOFs synthesized by hydrothermal or microwave methods at 180 °C could also be compounded with Yeast as a base material. This provides more possibilities that heavy metal ions are adsorbed by the synthesis of more diverse MOFs composites.

1. Introduction

Metal-organic frameworks (MOFs) are a kind of porous coordination polymers emerging in recent years [1]. The structural primitives of the MOFs can be different metal ions or clusters, and the organic reunion ligands also have different sizes, shapes and different coordination structures [2]. Therefore, the structure of the MOFs compound formed by the coordination bond is diverse. MOFs have high porosity and specific surface area [3], and can be used to in carbon dioxide capture [4], gas adsorption and separation [5], catalysis [6], and even biomedicine [7].

Meanwhile, MOFs also have some drawbacks. The chemical stability of MOFs is often lower than that of conventional porous carbon materials [8]. For example, some MOFs have the very high sensitivity to moisture [9], and the poor stability to acids and bases [10]. Those limit the range of applications of MOFs [11]. In order to overcome the shortcomings and rich applications, choosing the right base material and MOFs for compounding is an effective method to realize the maximum functionalization of MOFs [12]. For example: Lei et al. prepared metal-organic frameworks@cellulose aerogels composite materials by in situ growth to removal of heavy metal ions in water [13]. Fang et al. successfully anchored CdS nanoparticles on the surface of Yeast by hydrothermal processes to remove methylene blue (MB) dyes from aqueous solutions [14]. Zheng et al. prepared TiO₂@yeast-carbon composite microspheres on the pyrolysis method to investigate the adsorption capacity for

cationic dye methylene blue (MB) and anionic dye congo red (CR) [15].

In this paper, Yeast was prepared as a substrate material by hydrothermal processes [16]. Then ZIF-67 was anchored on the surface of Yeast by in situ growth at room temperature [17]. The mechanism of formation process of the ideal composite ZIF-67@Yeast is shown in Fig. 1 [14]. The prepared ZIF-67@Yeast was characterized in detail by SEM, BET, XRD and TG analysis. In addition, the adsorption properties of Pb²⁺ by ZIF-67@Yeast and the effect of initial concentration of Pb²⁺ on the adsorption and removal rate of Pb²⁺ by ZIF-67@Yeast were also investigated.

2. Experimental section

2.1. Materials

Highly active dry yeast was provided by Angel Yeast Co, Ltd. (Yichang, China). Glucose (plant cell culture grade), cobalt nitrate hexahydrate, dimethylimidazole (>98%), formaldehyde, methanol, ethanol were purchased from Aladdin Biochemical Technology Co, Ltd.

2.2. Synthesis

2.2.1. Synthesis of Yeast

Synthesis of Yeast based on references [16]. In a typical procedure,

* Corresponding author.

E-mail address: jkao@zstu.edu.cn (J. Gao).

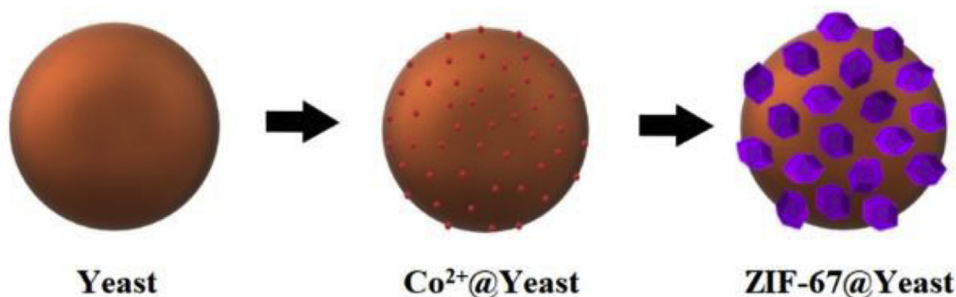


Fig. 1. The mechanism of formation process of ZIF-67@Yeast

10 g of yeast powder was added in 1 L of 1 wt% glucose solution, followed by stirring for 10 min, and putted it in a constant temperature oven at 37 °C for 1 h. Then the yeast solution was washed three times with a mixed solution of ethanol and water (water: ethanol = 1:1). After that the centrifuged yeast was added to 200 mL of a 4 wt% formaldehyde solution, followed by stirring for 10 min, and putted it in the hydrothermal kettle and reacted at 180 °C for 5 h. Finally, the hydrothermally carbonized yeast was centrifuged three times with a mixed solution of ethanol and water (water: ethanol = 1:1), and dried at 60 °C for 12 h to prepare the carbonized Yeast sample.

2.2.2. Synthesis of ZIF-67@Yeast

Synthesis of ZIF-67@Yeast based on references [17]. 0.87 g of $\text{Co}(\text{NO}_3)_2 \cdot 6\text{H}_2\text{O}$ was added to 30 mL of methanol, followed by stirring for 10 min, and added 200 mg of Yeast sample, followed by stirring for 12 h. Then centrifuged the mixture, and the centrifuged yeast was added to 200 mL of dimethylimidazole methanol solution (1.97 g dimethylimidazole + 20 mL methanol), followed by stirring for 6 h. Finally, the yeast solution was washed three times with methanol solution, and dried at 60 °C for 12 h to prepare the ZIF-67@ Yeast.

2.3. Characterization

The morphology of samples was observed by using field emission scanning electron microscopy (FESEM, Hitachi S4800, Japan). The crystal structure of samples was analyzed by using X-ray diffraction (XRD, Bruker D8, Germany) with $\text{Cu K}\alpha$ radiation (40 mA and 40 kV) at a scan rate of 3° min^{-1} . The surface areas of samples was calculated by using Brunauer-Emmett-Teller (BET, 3H-2000 PSI, China). The thermal stability of samples was characterized by using thermogravimetric analyzer (TGA, TG 209 F1, Germany) under a nitrogen atmosphere at a heating rate of $20^\circ \text{ C min}^{-1}$ and a temperature of 30–700 °C. Measurement of adsorption of Pb^{2+} by MOF composites by flame atomic absorption spectrometry (AAS, Spectr AA-220, USA).

2.4. Adsorption experiment

50 mL of three solution (Pb^{2+} concentration 100 ppm) were added to three 100 mL beakers, and 50 mg of Yeast sample was added to the beakers. The mixture solution was sonicated for 2 min, then the samples were taken from the solution at various time of 0.5, 1, 2, 4, 8 and 18 h and conducted metal ion concentration by using AAS. The same as ZIF-67 and ZIF-67@ Yeast.

3. Results and discussion

3.1. SEM analyses

The images of surface morphology of Yeast and ZIF-67@Yeast are shown in Fig. 2. Fig. 2(a) and (b) display the Yeast sample in different magnifications, which are shown that the hydrothermal carbonization of

Yeast at 180 °C is uniform spherical and uniform size (1–2 μm). Fig. 2(a) reveals that the Yeast possessed excellent mono-disperse performance. Fig. 2(b) expresses the detailed information of surface morphology of Yeast under a higher magnification. There are many small pores with uneven size on the surface, which are produced after the cytoplasmic efflux of the carbonization process. These pores may provide a suitable location for the growth of ZIF-67. Fig. 2(c) and (d) display ZIF-67@Yeast in different magnifications, which are shown that ZIF-67@Yeast is uniform spherical and uniform size (2 μm). Fig. 2 (d) expresses the detailed information of surface morphology of Yeast under a higher magnification. ZIF-67 random uniform adorned on the surface of Yeast as a monolayer. Thence, the ZIF-67@Yeast in Fig. 2(d) appears a typical raspberry-like structure. Additionally, it can be clearly observed that some residual areas still remained, which may have the enhancement for the adsorption of some metal ions in aqueous solution. Due to the large amount of anchorage of ZIF-67, an increase in the specific surface area of Yeast facilitates the adsorption of some metal ions in aqueous solution. Furthermore, the BET test results of Yeast and ZIF-67@Yeast are generalized in Fig. S1 and Table S1 (Supporting Information) [3c, 18]. As can be seen from Fig. S1, Yeast is a type III isotherm and ZIF-67@Yeast is a type I isotherm [19]. The specific surface area of Yeast and ZIF-67@Yeast are $7.1048 \text{ m}^2 \text{ g}^{-1}$ and $1644.8435 \text{ m}^2 \text{ g}^{-1}$ respectively. This further proves that it is because the anchoring of ZIF-67 greatly increases the specific surface area of ZIF-67@Yeast.

3.2. XRD analyses

XRD patterns of Yeast, ZIF-67 and ZIF-67@Yeast are shown in Fig. 3 (a). It is apparent from Fig. 3 (a) that the diffraction peaks(5.9° , 9.0° , 11.3° , 13.4° , 14.6°) of ZIF-67@Yeast is highly fit to those if the simulated ZIF-67. The peak of ZIF-67@Yeast is reduced because of the composite of Yeast. This shows that ZIF-67 were successfully obtained through synthesis process and mounted on the surface of Yeast. Again, in addition to the peak of ZIF-67 in ZIF-67@Yeast, no other peaks were detected, which indicates the high purity of ZIF-67@Yeast sample.

3.3. TG analyses

Fig. 3 (b) is the TGA curve for Yeast, ZIF-67 and ZIF-67@Yeast. ZIF-67 loading rate on Yeast was tested using Yeast and ZIF-67 for complete thermal decomposition temperatures. ZIF-67 has a high load rate on Yeast, reaching 31 wt%. After loading the ZIF-67 on the organic matrix material, the thermal properties of the composite are improved. Because the complete decomposition temperature of ZIF-67 is higher than that of organic materials. When the ZIF-67 was coated on the surface of the organic material, the substrate material is protected. Therefore, the thermal properties of the substrate material are improved. Furthermore, the thermal parameters are generalized in Table S2 (Supporting Information). Compared to Yeast, the maximum decomposition temperature (T_{\max}), initial decomposition temperature (T_0) and complete decomposition temperature (T_f) of ZIF-67@Yeast increased by 47.3°C , 51.8°C

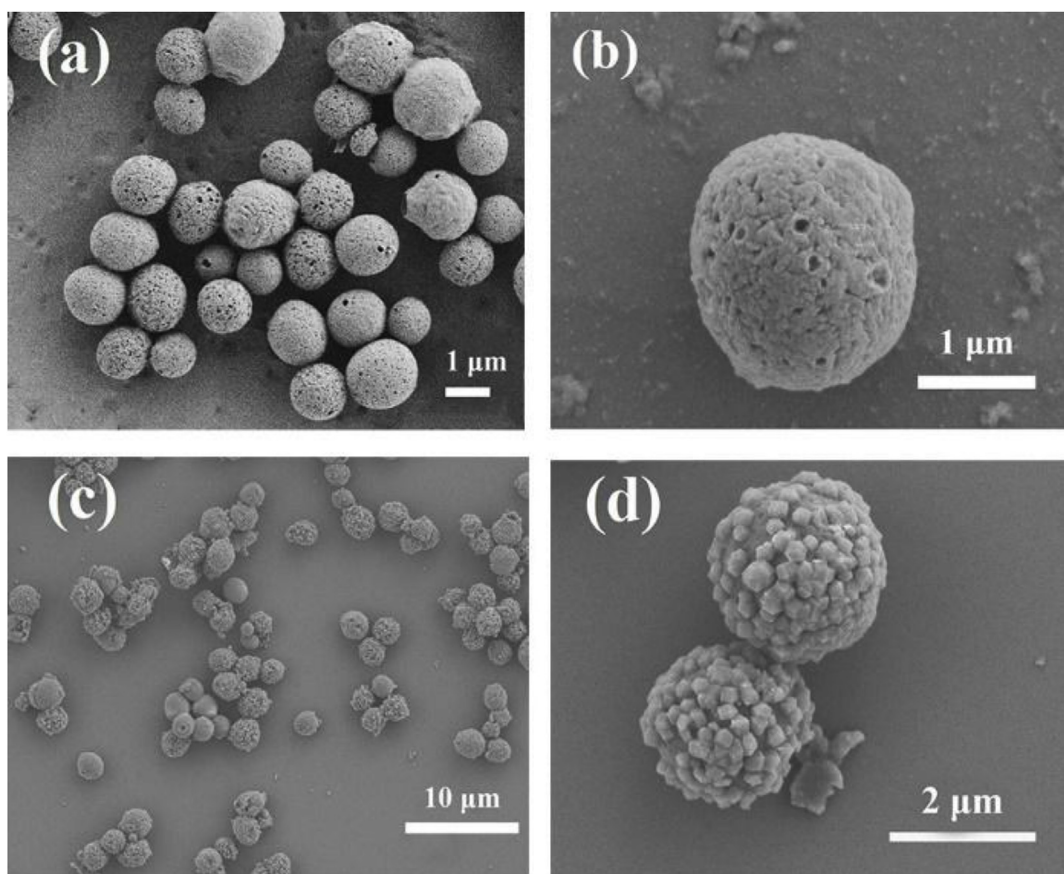


Fig. 2. SEM images of (a, b) Yeast, (c, d) ZIF-67@Yeast.

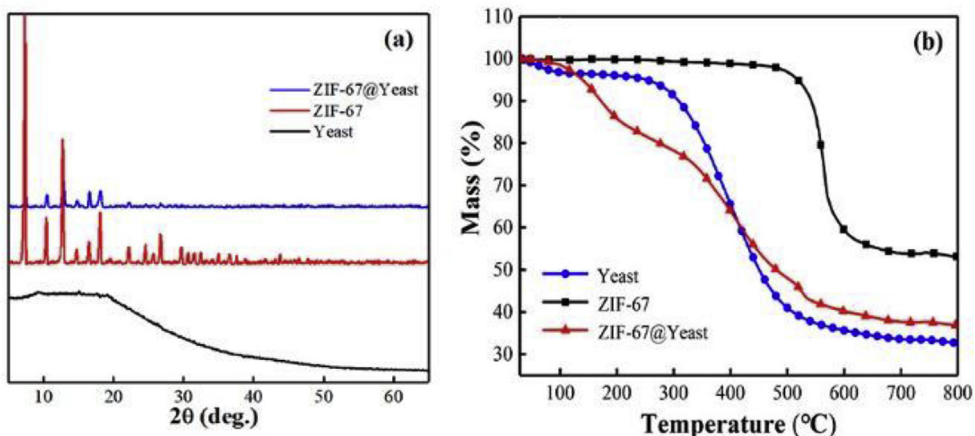


Fig. 3. (a) XRD patterns of Yeast, ZIF-67 and ZIF-67@Yeast, (b) TGA curves for Yeast, ZIF-67 and ZIF-67@Yeast.

and 37.7 °C. This further supports that the thermal stability of Yeast was improved by compounding.

3.4. Adsorption performance analysis

3.4.1. Adsorption performance of yeast, ZIF-67 and ZIF-67@Yeast

The equilibrium adsorption capacity of Pb^{2+} by Yeast, ZIF-67 and ZIF-67@Yeast was investigated, and the adsorption equilibrium curve and adsorption capacity are shown in Fig. 4 (a) and (b). The adsorption capacity of Pb^{2+} by Yeast is low at 11.09 mg g^{-1} . The adsorption capacity of Pb^{2+} by ZIF-67 is larger than Yeast at 50.1 mg g^{-1} . The adsorption capacity of Pb^{2+} by ZIF-67@Yeast is larger than that of Yeast and ZIF-67 at

62.5 mg g^{-1} , which is even slightly larger than the sum of the adsorption capacity of Pb^{2+} by Yeast and ZIF-67. This may be due to the fact that ZIF-67@Yeast has a large specific surface area, which increases contact with Pb^{2+} and facilitates absorption Pb^{2+} .

3.4.2. Adsorption kinetic of ZIF-67@Yeast

In order to explore the adsorption kinetic of ZIF-67@Yeast adsorbed Pb^{2+} , two kinetic models were established [20]. The linear formula of adsorption kinetic is as follows:

$$\ln(q_e - q_t) = \ln q_e - k_1 t \quad (1)$$

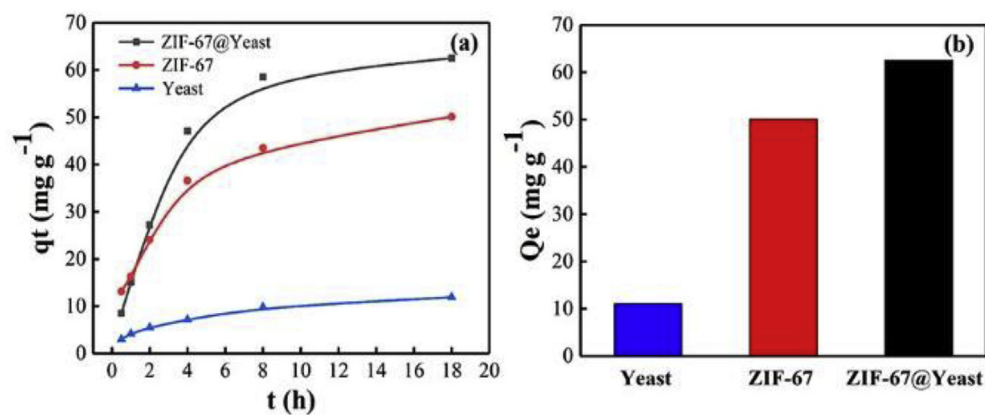


Fig. 4. (a) The adsorption equilibrium curve of Pb^{2+} by Yeast, ZIF-67 and ZIF-67@Yeast, (b) The adsorption capacity of Pb^{2+} by Yeast, ZIF-67 and ZIF-67@Yeast.

$$\frac{t}{q_t} = \frac{1}{k_2 q_e^2} + \frac{t}{q_e} \quad (2)$$

The linear formula (1) and (2) respectively represent pseudo-first-order kinetics model and pseudo-second-order kinetics model, which k_1 and k_2 respectively are the rate constants. The two kinetic models are shown in Fig. 5. The linear correlation coefficient R^2 of pseudo-second-order kinetics model of ZIF-67@Yeast adsorbed Pb^{2+} is 0.987, and the same of pseudo-first-order kinetics model is 0.8206 (Table S3). It is obvious that the linear correlation coefficient R^2 value of the second-order kinetics is larger than that of the first-order kinetics. This

indicates that the second-order kinetics are more reasonable, and the pseudo-second-time kinetics model of the adsorption time and the adsorption rate constant is more in line with the actual adsorbed situation.

3.4.3. Effect of initial concentration on adsorption capacity and removal rate

Three initial concentrations (100 ppm, 50 ppm and 10 ppm) were established to investigate the effect of the initial concentration of Pb^{2+} on the adsorption capacities and removal rates of ZIF-67@Yeast. The results are shown in Fig. 6. As can be seen from Fig. 6 (a), the adsorption capacities of Pb^{2+} by ZIF-67@Yeast increases as the initial concentration increases. At the same time of the first 4 h, the adsorption rate of 100 ppm is the largest and the lowest is 10 ppm. The adsorption equilibrium was reached after 4 h at 10 ppm, which was reached after 8 h at 100 ppm and 50 ppm. In Fig. 6 (b), the removal rates of Pb^{2+} by ZIF-67@Yeast decreases as the initial concentration increases. At the same time, the removal rate of 10 ppm is the largest and the lowest is 100 ppm. In terms of the amount of Pb^{2+} removed, 100 ppm is the largest yet.

4. Conclusions

ZIF-67@Yeast was successfully prepared with in-situ growth procedure by using hydrothermally carbonized yeast as the substrate material. ZIF-67 random uniform adorned on the surface of Yeast as a monolayer, which has a high load rate reaching 31 wt%. Compared with Yeast, the thermal stability of ZIF-67@Yeast was improved. The adsorption capacity of Pb^{2+} by ZIF-67@Yeast is larger than that of Yeast and ZIF-67 at 62.5 mg g^{-1} , which even slightly larger than the sum of the adsorption capacity of Pb^{2+} by Yeast and ZIF-67. A higher initial

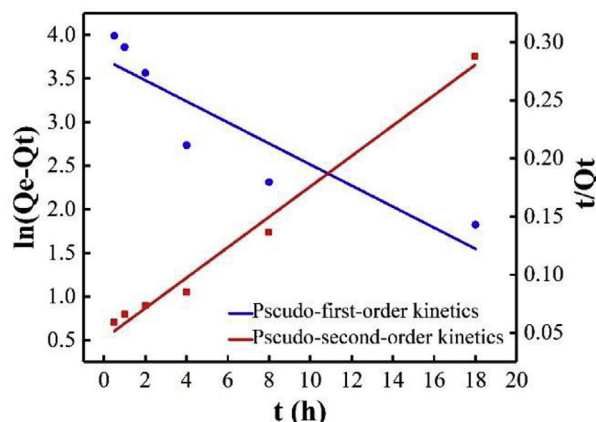


Fig. 5. Kinetic models of ZIF-67@Yeast adsorbed Pb^{2+} .

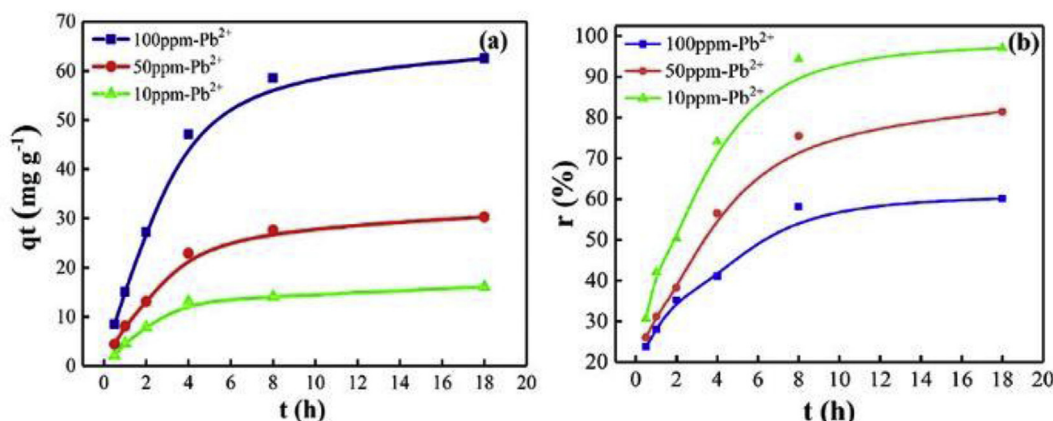


Fig. 6. (a) The adsorption capacities of different initial concentrations, (b) The removal rates of different initial concentrations.

concentration is more favorable for the adsorption of Pb^{2+} by ZIF-67@Yeast, and a lower initial concentration is more favorable for the removal of Pb^{2+} by ZIF-67@Yeast. Yeast could maintain a stable morphology after hydrothermal carbonization at 180 °C. Therefore, many MOFs synthesized by hydrothermal or microwave methods at 180 °C could also be compounded with Yeast as a base material. This provides more possibilities that heavy metal ions are adsorbed by the synthesis of more diverse MOFs composites.

Acknowledgements

This work was supported by the National Natural Science Foundation of China (51672251) and Science Foundation of Zhejiang Sci-Tech University (ZSTU) under Grant No. 13012138-Y.

Appendix A. Supplementary data

Supplementary data to this article can be found online at <https://doi.org/10.1016/j.jssc.2019.03.011>.

References

- [1] a) Q.L. Zhu, Q. Xu, Metal-organic framework composites, *Chem. Soc. Rev.* 43 (16) (2014) 5468–5512;
- b) J. Gao, K. Ye, L. Yang, W.-W. Xiong, L. Ye, Y. Wang, Q. Zhang, Growing crystalline zinc-1, 3, 5-benzenetricarboxylate metal-organic frameworks in different surfactants, *Inorg. Chem.* 53 (2014) 691–693;
- c) J. Gao, J. Miao, P.-Z. Li, W.Y. Teng, L. Yang, Y. Zhao, B. Liu, Q. Zhang, A p-type Ti (IV)-based metal-organic framework with visible-light photo-response, *Chem. Commun.* 50 (2014) 3786–3788.
- [2] a) J.D. Evans, B. Garai, H. Reinsch, W. Li, S. Dissegna, V. Bon, I. Senkovska, R.A. Fischer, S. Kaskel, C. Janiak, N. Stock, D. Volkmer, Metal-organic frameworks in Germany: from synthesis to function, *Coord. Chem. Rev.* 380 (2019) 378–418;
- b) P. Li, F.-F. Cheng, W.-W. Xiong, Q. Zhang, New synthetic strategies to prepare metal-organic frameworks, *Inorg. Chem. Front.* 5 (2018) 2693–2708;
- c) W.W. Xiong, Q. Zhang, Surfactants as promising media for the preparation of crystalline inorganic materials, *Angew. Chem. Int. Ed.* 54 (2015) 11616–11623;
- d) W.-W. Xiong, J. Miao, K. Ye, Y. Wang, B. Liu, Q. Zhang, Threading chalcogenide layers with polymer chains, *Angew. Chem. Int. Ed.* 54 (2015) 546–550;
- e) D.-D. Yang, Y. Song, B. Zhang, N.-N. Shen, G.-L. Xu, W.-W. Xiong, X.-Y. Huang, Exploring the surfactant-thermal synthesis of crystalline functional thioarsenates, *Cryst. Growth Des.* 18 (2018) 3255–3262;
- f) W.-W. Xiong, P.-Z. Li, T.-H. Zhou, A.I.Y. Tok, R. Xu, Y. Zhao, Q. Zhang, Kinetically controlling phase transformations of crystalline mercury selenidostannates through surfactant media, *Inorg. Chem.* 52 (2013) 4148–4150;
- g) W.-W. Xiong, G. Zhang, Q. Zhang, New strategies to prepare crystalline chalcogenides, *Inorg. Chem. Front.* 1 (2014) 292–301;
- h) W.-W. Xiong, E.U. Athresh, Y.T. Ng, J. Ding, T. Wu, Q. Zhang, Growing crystalline chalcogenidoarsenates in surfactants: from zero-dimensional cluster to three-dimensional framework, *J. Am. Chem. Soc.* 135 (2013) 1256–1259.
- [3] a) O.K. Farha, I. Eryazici, N.C. Jeong, B.G. Hauser, C.E. Wilmer, A.A. Sarjeant, R.Q. Snurr, S.T. Nguyen, A.O. Yazaydin, J.T. Hupp, Metal-organic framework materials with ultrahigh surface areas: is the sky the limit? *J. Am. Chem. Soc.* 134 (36) (2012) 15016–15021;
- b) Y.K. Park, S.B. Choi, H. Kim, K. Kim, B.H. Won, K. Choi, J.S. Choi, W.S. Ahn, N. Won, S. Kim, D.H. Jung, S.H. Choi, G.H. Kim, S.S. Cha, Y.H. Jhon, J.K. Yang, J. Kim, Crystal structure and guest uptake of a mesoporous metal-organic framework containing cages of 3.9 and 4.7 nm in diameter, *Angew. Chem. Int. Ed. Engl.* 46 (43) (2007) 8230–8233;
- c) I. Senkovska, S. Kaskel, Ultrahigh porosity in mesoporous MOFs: promises and limitations, *Chem. Commun.* 50 (54) (2014) 7089–7098;
- d) H. Xu, J. Gao, X. Qian, J. Wang, H. He, Y. Cui, Y. Yang, Z. Wang, G. Qian, Metal-organic framework nanosheets for fast-response and highly sensitive luminescent sensing of Fe^{3+} , *J. Mater. Chem. A* 4 (2016) 10900–10905.
- [4] a) J. Liu, P.K. Thallapally, B.P. McGrail, D.R. Brown, J. Liu, Progress in adsorption-based CO_2 capture by metal-organic frameworks, *Chem. Soc. Rev.* 41 (6) (2012) 2308–2322;
- b) A.A. Olajire, Synthesis chemistry of metal-organic frameworks for CO_2 capture and conversion for sustainable energy future, *Renew. Sustain. Energy Rev.* 92 (2018) 570–607;
- c) K. Cheng, Y. Li, Z. Gao, F. Chen, C. You, B. Sun, Two-dimensional metal organic framework for effective gas absorption, *Inorg. Chem. Commun.* 101 (2019) 27–31;
- d) B. Wang, A.P. Cote, H. Furukawa, M. O'Keeffe, O.M. Yaghi, Colossal cages in zeolitic imidazolate frameworks as selective carbon dioxide reservoirs, *Nature* 453 (7192) (2008) 207–211.
- [5] Y. He, W. Zhou, G. Qian, B. Chen, Methane storage in metal-organic frameworks, *Chem. Soc. Rev.* 43 (16) (2014) 5657–5678.
- [6] a) S.M.J. Rogge, A. Bavykina, J. Hajek, H. Garcia, A.I. Olivos-Suarez, A. Sepulveda-Escribano, A. Vimont, G. Clet, P. Bazin, F. Kapteijn, M. Daturi, E.V. Ramos-Fernandez, I.X.F.X. Llabres, V. Van Speybroeck, J. Gascon, Metal-organic and covalent organic frameworks as single-site catalysts, *Chem. Soc. Rev.* 46 (11) (2017) 3134–3184;
- b) J. Wang, J. Cong, H. Xu, J. Wang, H. Liu, M. Liang, J. Gao, Q. Ni, J. Yao, Facile gel-based morphological control of $Ag/g-C_3N_4$ porous nanofibers for photocatalytic hydrogen generation, *ACS Sustain. Chem. Eng.* 5 (2017) 10633–10639;
- c) Y. Wu, M. Lu, Y. Li, P. He, S.B. Maddine, J. Gao, J. Yao, Folic acid derived bimetallic-doped hollow carbon nanostructures for efficient electrocatalytic oxygen evolution, *Chem. Asian J.* 13 (2018) 3274–3280;
- d) J. Cong, H. Xu, M. Lu, Y. Wu, Y. Li, P. He, J. Gao, J. Yao, S. Xu, Two-dimensional Co@N-Carbon nanocomposites facilely derived from MOF nanosheets for efficient bifunctional electrocatalysis, *Chem. Asian J.* 13 (2018) 1485–1491;
- e) J. Gao, J. Cong, Y. Wu, L. Sun, J. Yao, B. Chen, Bimetallic hofmann-type metal-organic framework nanoparticles for efficient electrocatalysis of oxygen evolution reaction, *ACS Appl. Energy Mater.* 1 (2018) 5140–5144.
- [7] W. Chen, C. Wu, Synthesis, functionalization, and applications of metal-organic frameworks in biomedicine, *Dalton Trans.* 47 (7) (2018) 2114–2133.
- [8] a) F. Llabresixamena, O. Casanova, R. Galiaissottauer, H. Garcia, A. Corma, Metal organic frameworks (MOFs) as catalysts: a combination of Cu^{2+} and Co^{2+} MOFs as an efficient catalyst for tetralin oxidation, *J. Catal.* 255 (2) (2008) 220–227;
- b) E.V. Ramos-Fernandez, M. Garcia-Domingos, J. Juan-Alcaniz, J. Gascon, F. Kapteijn, MOFs meet monoliths: hierarchical structuring metal organic framework catalysts, *Appl. Catal. A Gen.* 391 (1–2) (2011) 261–267;
- c) W. Ren, J. Gao, C. Lei, Y. Xie, Y. Cai, Q. Ni, J. Yao, Recyclable metal-organic framework/cellulose aerogels for activating peroxyomonosulfate to degrade organic pollutants, *Chem. Eng. J.* 349 (2018) 766–774;
- d) J. Cong, C. Li, T. Zhao, J. Wu, R. Zhang, W. Ren, S. Wang, J. Gao, Y. Liu, J. Yao, Coordination polymer derived cobalt embedded in nitrogen-doped carbon nanotubes for efficient electrocatalysis of oxygen evolution reaction, *J. Solid State Chem.* 253 (2017) 227–230;
- e) H. Xu, S. Sommer, N.L.B. Nyborg, J. Gao, B.B. Iversen, The Chemistry of Nucleation: in situ Pair Distribution Function analysis of secondary building units during $UiO-66$ MOF formation, *Chem. Eur. J.* 25 (2019) 2051–2058.
- [9] a) J.A. Greathouse, M.D. Allendorf, The interaction of water with MOF-5 simulated by molecular dynamics, *J. Am. Chem. Soc.* 128 (33) (2006) 10678–10679;
- b) J. Kim, S. Yeo, J.-D. Jeon, S.-Y. Kwak, Enhancement of hydrogen storage capacity and hydrostability of metal-organic frameworks (MOFs) with surface-loaded platinum nanoparticles and carbon black, *Microporous Mesoporous Mater.* 202 (2015) 8–15.
- [10] J. Canivet, A. Fateeva, Y. Guo, B. Coasne, D. Farrusseng, Water adsorption in MOFs: fundamentals and applications, *Chem. Soc. Rev.* 43 (16) (2014) 5594–5617.
- [11] B.M. Connolly, J.P. Mehta, P.Z. Moghadam, A.E.H. Wheatley, D. Fairén-Jimenez, From synthesis to applications: metal-organic frameworks for an environmentally sustainable future, *Curr. Opin. Green Sustain. Chem.* 12 (2018) 47–56.
- [12] W. Ren, J. Gao, C. Lei, Y. Xie, Y. Cai, Q. Ni, J. Yao, Recyclable metal-organic framework/cellulose aerogels for activating peroxyomonosulfate to degrade organic pollutants, *Chem. Eng. J.* 349 (2018) 766–774.
- [13] C. Lei, J. Gao, W. Ren, Y. Xie, S.Y.H. Abdalkarim, S. Wang, Q. Ni, J. Yao, Fabrication of metal-organic frameworks/cellulose aerogels composite materials for removal of heavy metal ions in water, *Carbohydr. Polym.* 205 (2019) 35–41.
- [14] F. Qin, B. Bai, D. Jing, L. Chen, R. Song, Y. Suo, CdS nanoparticles anchored on the surface of yeast via a hydrothermal processes for environmental applications, *RSC Adv.* 4 (66) (2014) 34864–34872.
- [15] Z. Pei, Z. Kaiqiang, D. Yu, B. Bo, G. Weisheng, S. Yourui, Adsorption of organic dyes by TiO_2 @yeast-carbon composite microspheres and their in situ regeneration evaluation, *J. Nanomater.* 2015 (2015) 1–13.
- [16] a) H. Sun, W. He, C. Zong, L. Lu, Template-free synthesis of renewable macroporous carbon via yeast cells for high-performance supercapacitor electrode materials, *ACS Appl. Mater. Interfaces* 5 (6) (2013) 2261–2268;
- b) D. Ni, L. Wang, Y. Sun, Z. Guan, S. Yang, K. Zhou, Amphiphilic hollow carbonaceous microspheres with permeable shells, *Angew. Chem. Int. Ed.* 49 (25) (2010) 4223–4227;
- c) Y. Xie, L. Fang, H. Cheng, C. Hu, H. Zhao, J. Xu, J. Fang, X. Lu, J. Zhang, Biological cell derived N-doped hollow porous carbon microspheres for lithium-sulfur batteries, *J. Mater. Chem. A* 4 (40) (2016) 15612–15620.
- [17] a) X. Li, Z. Li, L. Lu, L. Huang, L. Xiang, J. Shen, S. Liu, D.R. Xiao, The solvent induced inter-dimensional phase transformations of cobalt zeolitic-imidazolate frameworks, *Chem. Eur. J.* 23 (44) (2017) 10638–10643;
- b) M. Wang, J. Liu, C. Guo, X. Gao, C. Gong, Y. Wang, B. Liu, X. Li, G.G. Gurzadyan, L. Sun, Metal-organic frameworks (ZIF-67) as efficient cocatalysts for photocatalytic reduction of CO_2 : the role of the morphology effect, *J. Mater. Chem. A* 6 (11) (2018) 4768–4775.
- [18] a) K.S. Walton, R.Q. Snurr, Applicability of the BET method for determining surface areas of microporous metal-organic frameworks, *J. Am. Chem. Soc.* 129 (27) (2007) 8552–8556;
- b) Y.S. Bae, A.O. Yazaydin, R.Q. Snurr, Evaluation of the BET method for determining surface areas of MOFs and zeolites that contain ultra-micropores, *Langmuir* 26 (8) (2010) 5475–5483;
- c) T.C. Wang, W. Bury, D.A. Gomez-Gualdrón, N.A. Vermeulen, J.E. Mondloch, P. Deria, K. Zhang, P.Z. Moghadam, A.A. Sarjeant, R.Q. Snurr, J.F. Stoddart, J.T. Hupp, O.K. Farha, Ultrahigh surface area zirconium MOFs and insights into the applicability of the BET theory, *J. Am. Chem. Soc.* 137 (10) (2015) 3585–3591;
- d) B. Streppel, M. Hirscher, BET specific surface area and pore structure of MOFs

- determined by hydrogen adsorption at 20 K, *Phys. Chem. Chem. Phys.* 13 (8) (2011) 3220–3222.
- [19] a) K.S. Sing, Reporting physisorption data for gas/solid systems with special reference to the determination of surface area and porosity (Recommendations 1984), *Pure Appl. Chem.* 57 (4) (1985) 603–619;
b) P.I. Ravikovitch, A.V. Neimark, Characterization of nanoporous materials from adsorption and desorption isotherms, *Colloids Surf., A* 187 (2001) 11–21;
- c) C. Hinz, Description of sorption data with isotherm equations, *Geoderma* 99 (3–4) (2001) 225–243.
- [20] a) Y.-S. Ho, G. McKay, Pseudo-second order model for sorption processes, *Process Biochem.* 34 (5) (1999) 451–465;
b) D. Shen, X. Ma, T. Cai, X. Zhu, X. Xin, Q. Kang, Investigation on kinetic processes of zeolitic imidazolate framework-8 film growth and adsorption of chlorohydrocarbons using a quartz crystal microbalance, *Anal. Meth.* 7 (22) (2015) 9619–9628.